692 *Journal of Mechanical Science and Technology (KSME Int. J.), Vol. 20, No. 5, pp. 692~709, 2006*

Experimental Study on Single Bubble Growth Under Subcooled, Saturated, and Superheated Nucleate Pool Boiling

Jeongbae Kim
New & Renewable Energy Research Department, KIER (Korea Institute of Energy Research), 71-2, Jang-dong, Yuseong-gu, Daejeon 305-343, Korea
Jangho Lee
Department of Mechanical Engineering, Kunsan National University, San 68, Miryong-dong, Kunsan, Jellabuk-do 573-701, Korea
Moo Hwan Kim*
Department of Mechanical Engineering, Pohang University of Science and Technology, San 31, Hyoja-dong, Namgu, Pohang, Kyoungbuk-do 790-784, Korea

Nucleate pool boiling experiments with constant wall temperature were performed using pure R113 for subcooled, saturated, and superheated pool conditions. A microscale heater array and Wheatstone bridge circuits were used to maintain the constant wall temperature and to measure the instantaneous heat flow rate accurately with high temporal and spatial resolutions. Images of bubble growth were taken at 5,000 frames per second using a high-speed CCD camera synchronized with the heat flow rate measurements. The bubble geometry was obtained from the captured bubble images. The effect of the pool conditions on the bubble growth behavior was analyzed using dimensionless parameters for the initial and thermal growth regions. The effect of the pool conditions on the heat flow rate behavior was also examined. This study will provide good experimental data with precise constant wall temperature boundary condition for such works.

Key Words : Pool Temperature, Constant Wall Temperature, Single Bubble Growth, Nucleate Pool Boiling, Microscale Heater Array

Nomenclature

A : Dimensional parameter for calculation of bubble volume
B : Dimensional parameter for calculation of bubble volume
C : Dimensional parameter for calculation of bubble volume
C_{P_1} : Liquid specific heat
D : Dimensional parameter for calculation of bubble volume
E : Dimensional parameter for calculation of bubble volume
h_{fg} : Latent heat for vaporization
Ja : Jakob number (defined by $(\rho_l C_{P_l} \Delta T)/(\rho_v h_{fg})$)
k_l : Liquid thermal conductivity
$\dot{m}$: Evaporating mass flow rate
q_{latent} : Latent heat transfer
$\dot{q}$: Heat flow rate
$\dot{q}^+$: Dimensionless heat flow rate
$\dot{q}_c$: Characteristic heat flow rate
$\dot{q}_{conduction}$: Conduction heat transfer rate through the interface
r : Radial direction
r^+ : Dimensionless radius

* Corresponding Author,
E-mail : mhkim@postech.ac.kr
TEL : +82-54-279-2165; **FAX** : +82-54-279-3199
Department of Mechanical Engineering, Pohang University of Science and Technology, San 31, Hyoja-dong, Namgu, Pohang, Kyoungbuk-do 790-784, Korea.
(Manuscript **Received** July 14, 2005; **Revised** February 20, 2006)

R : Radius or Equivalent bubble radius
R_c : Characteristics bubble radius scale
R_d : Departure bubble radius
R_{eq} : Equivalent bubble radius
R^+ : Dimensionless bubble radius
t : Time
t_c : Characteristics time scale
t_w : Waiting time
t^+ : Dimensionless time
Δt : Time difference
Δt^+ : The variation of the characteristic time
T : Temperature
T_b : Bulk liquid temperature (or pool temperature)
T_c : Characteristic temperature scale
T_{sat} : Saturation temperature
T_{wall} : Wall temperature
V : Total bubble volume
v_{cL} : Characteristic velocity scale
V_L : Bubble volume of the lower part
V_U : Bubble volume of the upper part

Greeks

α : Liquid thermal diffusivity
ΔT : Wall superheat (defined by $T_{wall}-T_{sat}$)
ΔP : Pressure potential
ρ_v : Vapor density
ρ_l : Liquid density
σ : Surface tension

1. Introduction

Many experiments and analyses have been performed to clarify the heat transfer mechanism of boiling. The overall characteristics of boiling are directly and indirectly influenced by the behavior of a single bubble on the heating surface. The heat transfer mechanism for single bubble growth can be related to the thermal boundary layer characteristics on the heating surface. These are controlled by the wall and pool temperatures during the waiting period, and by the interface temperature gradient, which is depended on wall, saturation, and pool temperatures during the growth time. Consequently, the temperature scales closely connected to nucleate pool boiling are the pool temperature (subcooled, saturated, and superheated), saturation temperature of the working fluid, and heating wall temperature.

Rayleigh (1917) proposed the momentum equation for a spherical bubble to be governed by the momentum interaction between the two phases without considering the heat transfer through the interface between the liquid and vapor bubble. Analytically, he showed that bubble radius was proportional to the growth time based on a constant pressure difference assumption. Plesset and Zwick (1954) and Forster and Zuber (1954) analyzed the extended Rayleigh equation considering the heat transfer through the bubble interface in a uniformly superheated liquid, and then derived a bubble growth equation using heat conduction through the thermal boundary layer. They assumed a thin thermal boundary layer and uniformly superheated liquid surrounding the vapor bubble, and derived the temperature distribution at the interface. Their analysis showed that the bubble radius increased proportionally with $t^{1/2}$. For a vapor bubble larger than a critical radius and surrounded by a uniformly superheated liquid, Mikic et al. (1970) analyzed the bubble growth behavior using characteristic length and time scales in a dimensional analysis. They reported that the bubble radius increased proportionally with t^1 for dimensionless time values much less than 1 ($t^+\ll 1$), and with $t^{1/2}$ for dimensionless time values much greater than 1 ($t^+\gg 1$). However, they did not categorize the bubble growth regions.

Robinson and Judd (2001) performed a numerical simulation of bubble growth based on interface temperature calculations using the extended Rayleigh and energy equations. They considered the inside vapor pressure of a hemispherical bubble attached on the heating surface and demonstrated that heat transfer occurred through the bubble interface due to the interface cooling effect previously proposed by Plesset and Zwick (1954), Zuber (1961), and Mikic et al. (1970). They divided the bubble growth regions based on their numerical results. When a bubble forms after a waiting period, the bubble growth is governed by the surface tension for a short period of time (surface-tension controlled region). As the bubble increases in volume, the surface tension is reduced while the inertia is increased (inertia controlled region). When the vapor pressure of the bubble is balanced with the system pressure, the temperature distribution at the interface of the two phases becomes the most important parameter for bubble growth (thermal growth region).

According to bubble radius results of Han and Griffith (1965) and Cole and Shulman (1966), performed at a constant heat flux condition for saturated pool boiling, there are the large deviations even when tests are performed under the same experimental conditions. These arise from the poor control capacity of the heating surface. Our analysis showed that the control speed of the heating surface must be only a few microseconds to maintain a constant heating condition from bubble inception to departure. Hooper and Abdelmessih (1966) and Sernas and Hooper (1969) performed nucleate pool boiling experiments using water with a constant heat flux condition and then studied the bubble growth behavior during the initial growth region. However, they compared their experimental results with the growth rate of $t^{1/2}$ obtained from the analytical results of Plesset and Zwick (1954) and Forster and Zuber (1954).

And previously, Lee et al. (2003a) reported that the growth rate in the thermal growth region varied as $t^{1/7}$ with the bubble growth result at only one wall superheat condition for saturated pool condition using R11, but fixed in the initial growth rate like t^1 as the propose of Rayleigh (1917). Then, Lee et al. (2003b) demonstrated that the bubble growth rate in the thermal growth region followed as $t^{1/5}$ with various wall superheats for just saturated pool condition using R11 and R113, but fixed in the initial growth rate with t1 as proposed by Rayleigh (1917). They used a Jakob number (Ja) based on the wall superheat (the difference between the wall and saturation temperatures) ranging from 14 to 21. Also reported that the thermal growth rate was regardless of the working fluid and heating conditions. Lee et al. (2004) showed that the growth behavior of binary mixtures in the thermal growth region for saturated pool condition was almost same as for pure substances.

In this study, we performed nucleate pool boiling experiments with fixed wall temperature using one fluid to examine pool temperature effects on the bubble growth behavior. In previous studies, it was almost impossible to maintain a constant fixed wall temperature for nucleate pool boiling under constant atmospheric pressure condition. Even for saturated and subcooled pool boiling, the heating surface condition used in most previous single bubble growth research was a constant heat flux that could be obtained by heating a metallic block installed below the bubble. There were large deviations in the bubble radius results of Han and Griffith (1965), Cole and Shulman (1966), and Zuber (1961), even when the experiments were performed under the same conditions. This resulted from the poor control capacity of the heating surface. A control speed of a few microseconds is required to respond to the local heating conditions and a fixed temperature during bubble formation.

Zuber (1961) proposed a growth and collapse equation using the maximum bubble radius and time under non-uniform temperature fields based on subcooled nucleate boiling results of Ellion. Demiray and Kim (2003) described the bubble growth behavior for subcooled boiling at 5℃ (low amount) and 15℃ (high amount) of subcooling under constant temperature condition using FC-72 (Tsat=56.7℃). In addition, Kim et al. (2002) published the effects of subcooling on the pool boiling heat transfer. However they did not fully describe the effects of the pool temperature on the bubble growth behavior.

For superheated pool condition, previous studies usually performed at an infinite pool, so that during growth, the bubble was not attached to the heating surface and there was no effect due to the waiting period between series of bubbles from inception to departure. Forster and Zuber (1954), Dergarabedian (1960), and Saddy and Jameson (1971) presented bubble growth rate and heat transfer results that considered the pool superheat effect at an infinite pool of water at atmospheric pressure. Their experimental pool conditions from

1 to 5℃ of pool superheat. Lien (1969) performed a similar study to study the bubble growth rate for 9 to 16℃ of superheat with a variable system pressure and an infinite pool. Van Stralen et al. (1975) studied the growth rate of a bubble attached to the heating surface until departure in a pool with 0.8 to 2.3℃ of superheat, also with a variable system pressure.

The objective of this study was to investigate the effect of only pool temperature conditions (superheated, saturated, and subcooled) on single bubble growth characteristics including bubble growth rates in initial and thermal growth regions under constant wall temperature and atmospheric pressure. To do so, the wall temperature was fixed using a microscale heater array with high temporal and spatial resolutions that was originally designed by Rule et al. (1998). And Lee et al. (2003a, 2003b, 2004) and Kim et al. (2004, 2005) also used the same microscale heater array.

To achieve our objective, nucleate pool boiling experiments were conducted for subcooled, saturated, and superheated pool conditions using pure R113 (T_{sat}=47.6℃). The wall temperature was maintained at a 72℃ for all the pool temperature conditions. For subcooled conditions, the pool temperature was set to 30, 32, 34, 36, 38, 40, 42, 44, and 45℃ to consider and include the subcooled range of Demiray and Kim (2003). For superheated conditions, the pool temperature was set to 48, 49, and 50℃. A pool temperature of 47℃ was considered as nearly saturated and used as the reference condition. When the pool temperature exceeded 50℃ and was lower than 30℃, regular single bubble events did not occur ; therefore, we could not obtain bubble images or measure the heat flow rate with a good degree of repeatability.

2. Experiments

2.1 Experimental apparatus

We used a microscale heater array to maintain a constant temperature at the heating surface and to measure the heat flow rate. The heater was fabricated on a transparent glass wafer using a very-large-scale-integrated (VLSI) technique. The transparency provided a bottom view of the growing bubble, which was captured using a high speed CCD camera. First, a titanium and platinum layer for the heater line on the wafer was installed using thermal evaporation. Then, a titanium and platinum layer for the power line was fabricated. The roughness of the heating surface was approximately 0.4 μm, which was the height of the heating line with respect to the base substrate. The static contact angle of the microscale heater array surface was 71° for distilled water and 11.4° for R113, which indicates the hydrophilic nature of R113. A total of 96 microscale heaters comprised one microscale heater array. Each microscale heater measured 0.27×0.27 mm^2, and the total size of the microscale heater array was 2.7×2.7 mm^2. For our experiments, the heater was manufactured at the Samsung Advanced Institute of Technology based on the idea of Rule et al. (1998) and Rule and Kim (1999). Most of the experimental devices that have been used previously to control the power of the heating block beneath the bubble, and thereby provide a constant heat flux, could not maintain a constant surface temperature over very short time intervals. However, Our microscale heater array was controlled with a Wheatstone bridge circuit that provided a constant surface temperature with a high temporal resolution. The longest time delay in the circuit occurred at the OP amp (LTC1150), which had a time resolution of 10^{-7} s. Due to the fast response of the circuitry, good repeatability was achieved in our experimental results. The temperature of the 96 heaters in the array was controlled by 96 electric Wheatstone bridge feedback circuits, which were operated in a manner similar to that used for constant-temperature hot-wire anemometry. Each heater in the array could be represented as one resistor in a Wheatstone bridge circuit, consisted of two fixed resistance, microscale heater, and digital potentiometer. The digital potentiometer (DS1267) is an actual controlling device that is used as a variable resistance.

The microscale heater has the linear relation between its resistance and temperature. The temperature of the microscale heater can be determined with its resistance that can be controlled by the potentiometer in the Wheatstone bridge circuit. The direct control parameter of the potentiometer is the digital number that means the proportional value to the maximum resistance of 20 kΩ. But the exact relationship between the digital number of the potentiometer and the temperature of the heater itself should be known before the experiments. So, to maintain and control the constant temperature condition, each heater was previously calibrated for temperatures ranging from 20 to 80℃. The digital numbers of each 96 heaters for a temperature are slightly different because the components of each circuit have different values and the resistances of the heaters at the same temperature are different. Therefore, to keep the microscale heater array at a certain wall temperature, the corresponding 96 digital numbers of the potentiometers should be known for each temperature. In order to find out the digital numbers for all 96 heaters, a constant temperature bath (HAAKE D8-G) was used. The constant temperature bath contained olive oil as a working fluid.

When a wall temperature was selected, the corresponding 96 digital numbers of the potentiometers memorized as file was put on. If the resistances of the microscale heater array, occurred from the temperature variation according to bubble inception, growth, and departure, changed, then OP amp begins to amplify the whole circuit voltage. The calibration process for the wall temperature of each heater was described in Lee et al. (2003b). A data acquisition system,

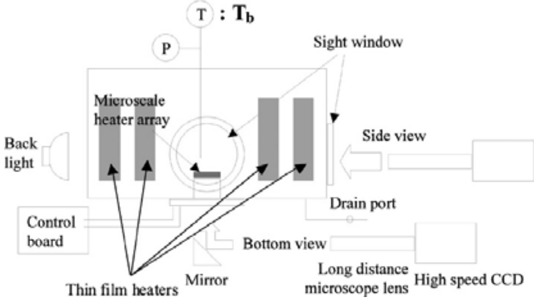

Fig. 1 Schematic diagram of the experimental apparatus

which could measure and store data at 7.35 kHz with 12-bit resolution, was used to measure the heat flow rate of each heater throughout the experiments. Therefore, the voltage data for each heater was sampled every 0.136 msec, and 1,000 voltage readings for each heater were stored with the 12-bit resolution. All the tests performed in this study lasts 136 msec. These measurements were synchronized with the images captured by the high speed CCD camera. A more detail description can be found in Rule and Kim (1999) and Bae et al. (1999). Fig. 1 shows a schematic diagram of the experimental apparatus. We used a RTD temperature sensor (OMEGA) located vertically about 50 mm apart from the center of the microscale heater array to measure the bulk temperature and use the reference scale, and used the commercial temperature controller. The about 50 mm distance was determined as the distance to neglect the temperature effect of the microscale heater array. And ten thin film heaters were used to control the liquid temperature inside the test chamber and attached at outside wall of the chamber that made by aluminum. Each of ten heaters has the capacity of 15,500 W/m^2. A 150 Watts cold light source was used for the CCD camera. The speed of CCD camera (Redlake Co., HG-100K) was 5,000 frames per second. A long distance microscopic lens was used to capture the small bubbles during boiling (see Fig. 1).

2.2 Uncertainty analysis

The bubble growth behavior was analyzed using side-view images, while the heat flow rate measured using the microscale heater during growth. Since most previous results for bubble growth have been for a spherical bubble, the growth behavior in this study was analyzed using the equivalent radius of a sphere with the same volume. The captured images showed reasonable bubble geometries, with an axi-symmetric shape about the vertical axis and a non-symmetric shape about the horizontal axis, as shown like Fig. 2. (Kim et al., 2004) Based on the shape assumption, we calculated the volume of upper and lower parts of the bubble using :

$$V_U=\frac{2}{3}\pi B^2 A \quad (1)$$

$$V_L=\pi B^2\left[D-\frac{D^3}{3E^2}\right],\ E=\sqrt{\frac{D^2}{1-\frac{(C/2)^2}{B^2}}} \quad (2)$$

where, A, B, C, D and E are the dimensions indicated in Fig. 2. V_L can also be calculated using B, D, and C (see Fig. 2). The equivalent radius, R_{eq}, can then be defined as the radius for which the total volume (V) from the measurements is balanced with that of a sphere with an equivalent radius,

$$V=V_U+V_L=\frac{4}{3}\pi R_{eq}^3 \quad (3)$$

$$R_{eq}=\left(\frac{1}{2}B^2 A+\frac{3}{4}B^2\left[D-\frac{D^3}{3E^2}\right]\right)^{\frac{1}{3}} \quad (4)$$

The heat flow rate supplied to the bubble corresponds to that required for the total bubble volume change based on the assumption that the volume change is induced by latent heat transfer. This can be calculated from

$$\dot{q}=\dot{m}h_{fg}=4\pi\rho_v h_{fg}R^2\frac{dR}{dt} \quad (5)$$

The equivalent radius can be calculated from the dimensions shown in Fig. 2 ; however, the errors in the dimensional measurements will propagate into the calculation of the equivalent radius. The dimensions shown in Fig. 2 were measured by counting the number of pixels in each captured image. A micrometer was placed in the chamber at the same distance as the bubble nucleation to provide guidance for the size measurements. From the captured micrometer images, a physical dimension of 1 mm corresponded to 197 pixels in our experiments. Therefore, one pixel in each image corresponded to 5.0761 μm. The clearly captured images could be measured with an error of ± 1 pixel. An uncertainty analysis was performed using the method described by Coleman and Steele (1989). The maximum uncertainty in the first image, which contained the smallest bubble, was 5.0%.

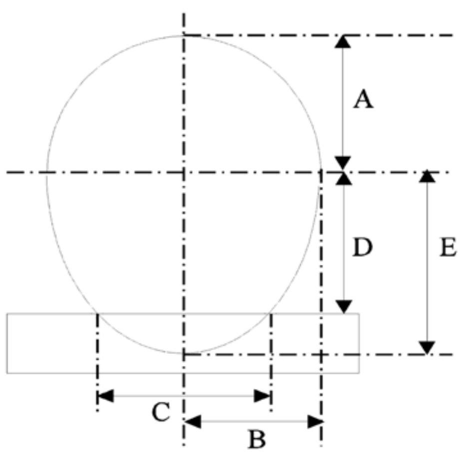

Fig. 2 Geometry of the spheroid used to determine the bubble volume

The bubble inception time was obtained from the time when the first image was recorded as indicated by the CCD camera, and from the heat flow rate data. The images were recorded with a time resolution of 0.2 msec (5,000 frames/sec). We defined the inception time was as the point immediately before the jump in the recorded heat flow rate data ; therefore, the inception time error was a maximum of 0.136 ms. A thermocouple with 0.53℃ uncertainty was used to calibrate the temperature of the microscale heater array. The Wheatstone bridge circuit was set to give a temperature displacement of 60℃ and the digital potentiometer in the Wheatstone bridge circuit had 512 digital positioning numbers. Therefore, one digit had a 0.12℃ temperature displacement and an uncertainty of 0.06℃. The maximum uncertainty of the calibrated temperature was estimated to be 0.59℃ which was the sum of the errors of the thermocouple and digital potentiometer : 0.53℃ and 0.06℃, respectively.

The voltage of each heater was measured using a 12-bit A/D system. The maximum voltage was 12 V. Therefore, the digitizing bias error was estimated to be ± 0.0015 V. All of the heater output voltages measured while a bubble was generated were above 2 V and the maximum uncertainty of the voltage measurements was $\pm 0.075\%$.

The temperature difference between the heating wall and pool was a maximum of 40℃ for the subcooled case with a pool temperature of 32℃. The difference in the refractive index of pure R113 is roughly 0.59% for a temperature difference of 40℃. The distortion or refraction error caused at the window or near the heating surface liquid, whose density differs from that of the bulk liquid, will be negligible. The data on the refractive index of pure R113 was obtained from page 18.3 of the 1997 Fundamentals of ASHRAE Handbook and page 1640 of the Handbook of Fine Chemicals and Laboratory Equipment of Sigma Aldrich Inc.

3. Results and Discussion

3.1 Measured heat flow rate uncertainty and bubble geometry

One of our objectives was to analyze the growth behavior of a single bubble by measuring the heat flow rate supplied from the heating wall under constant wall temperature condition for each pool temperature. Therefore, the uncertainty of the measured heat flow rate at the microscale heater is important. To evaluate the uncertainty of all the experiments conducted in this study, we examined the measured heat flow rate behavior in Fig. 3. Fig. 3 shows the heat flow rate behavior of the measured cycles for 32, 42, 47, and 49℃. The maximum error arises from the 0.136 msec in the bubble inception time measurements due to the time resolution of the heat flow rate. After an initial peak and an abrupt decrease, the heat flow rates showed good repeatability with deviations of 4%. This suggests that the bubble behavior will be similar for each period between inception and departure.

In order to verify the assumed bubble geometry, which was used to obtain the equivalent bubble radius, we inspected the bubble shapes during growth using captured image, such as those shown in Fig. 4. The images showed bubbles that were

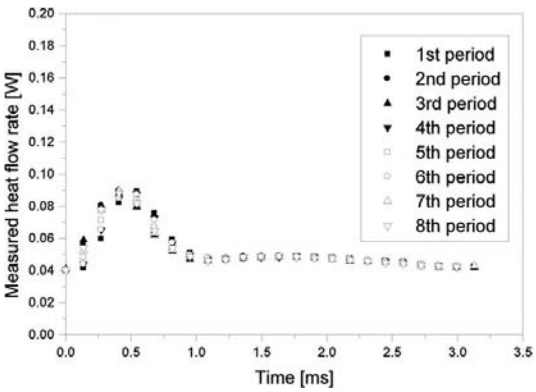

(a) T_b=32℃

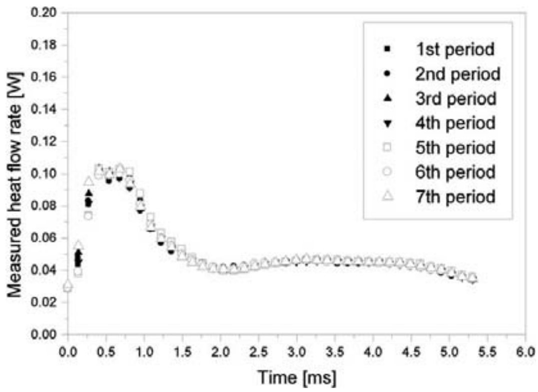

(b) T_b=42℃

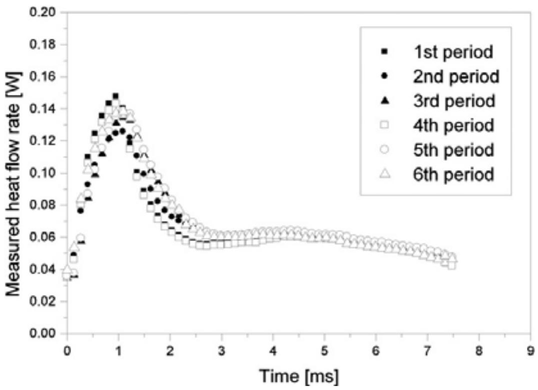

(c) T_b=47℃

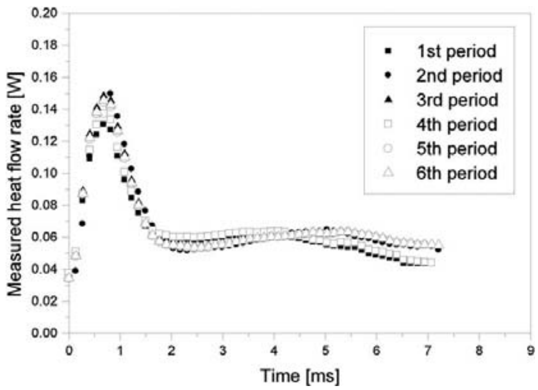

(d) T_b=49℃

Fig. 3 Repeatability of the measured heat flow rate almost axi-symmetric about the axis normal to the heating surface, but not symmetric about the horizontal axis, regardless of the pool temperature conditions. These images were compared to the bubble geometry illustrated in Fig. 2. A necking phenomenon occurred close to the departure time, resulting in a difference between the assumed shapes and the actual images. The maximum difference appeared right at the departure time. To evaluate the equivalent radius of the actual bubble, the coordinates of the bubble interface were measured and integrated to obtain the volume. The equivalent radius evaluated from the actual volume at the departure time for a pool temperature of 47℃ pool temperature was 0.589 mm, and the equivalent radius evaluated from the assumed shape at the same time was 0.612 mm. Therefore, the estimated maximum error in the assumed shape was 3.8%.

Figure 5 gives values of the dimensions A, B, C, and D, which were illustrated in Fig. 2 for bubbles under various pool conditions. Here, A is the height of the upper part, B is the maximum radius, C is the contact diameter, and D is the height of the lower part. Except for a pool temperature of 32℃, which was a highly subcooled case, the characteristics of the bubble geometries for different pool conditions were very similar.

The estimated equivalent bubble radius for each pool temperature is shown in Fig. 6. Fig. 6 indicates that the larger bubble, the greater the pool temperature. For subcooled conditions ranging from 38 to 45℃, the bubble radius did not decrease until departure, although the pool tem-

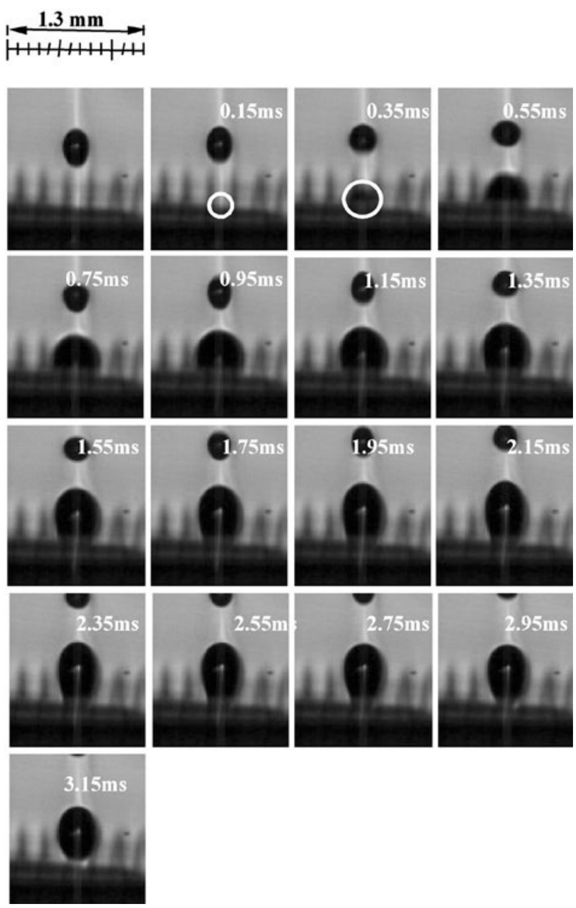

(a) $T_b=32℃$

Fig. 4 Side view images of bubble growth ($T_b=32℃$, 47℃, and 49℃)

perature was less than the saturation temperature. The bubble radius decreased for pool temperatures less than 36℃, and a negative growth rate was observed for pool temperatures of 32 and 34℃. For superheated conditions ranging from 48 to 49℃, the bubble growth rate was greater than that of the almost saturated case at 47℃.

The equivalent radius of the saturated pool condition with a temperature of 47℃ is compared wirh previous analytical results in Fig. 7(a). Plesset and Zwick (1954) assumed a uniformly superheated thermal boundary layer around the spherical bubble and predicted a $t^{1/2}$ asymptotic growth rate as Eq. (6).

$$R(t)=\sqrt{\frac{12}{\pi}}\mathrm{Ja}\sqrt{\alpha t} \quad (6)$$

Other predictions that modified using the effective heat transfer area (Van Stralen, 1966) and considered the non-uniform temperature field around the bubble (Mikic and Rohsenow, 1969) still give that the bubble grows with an asymptotic growth rate of approximately $t^{1/2}$ as Eqs. (7) and (8), respectively.

$$R=0.7\left(\frac{12}{\pi}\right)^{1/2}\mathrm{Ja}(\alpha t)^{1/2} \quad (7)$$

$$R=2\frac{\sqrt{3}}{\pi}\mathrm{Ja}\sqrt{\pi\alpha t}\left\{1-\frac{T_{wall}-T_b}{T_{wall}-T_{sat}}\left[\left(1+\frac{t_w}{t}\right)^{1/2}-\left(\frac{t_w}{t}\right)^{1/2}\right]\right\} \quad (8)$$

However, our results showed two different regions between bubble inception and departure. Before 1 msec, the growth rate in the initial growth region was proportional to $t^{2/3}$, as proposed by Kim et al. (2005); after 1 msec, the growth rate in

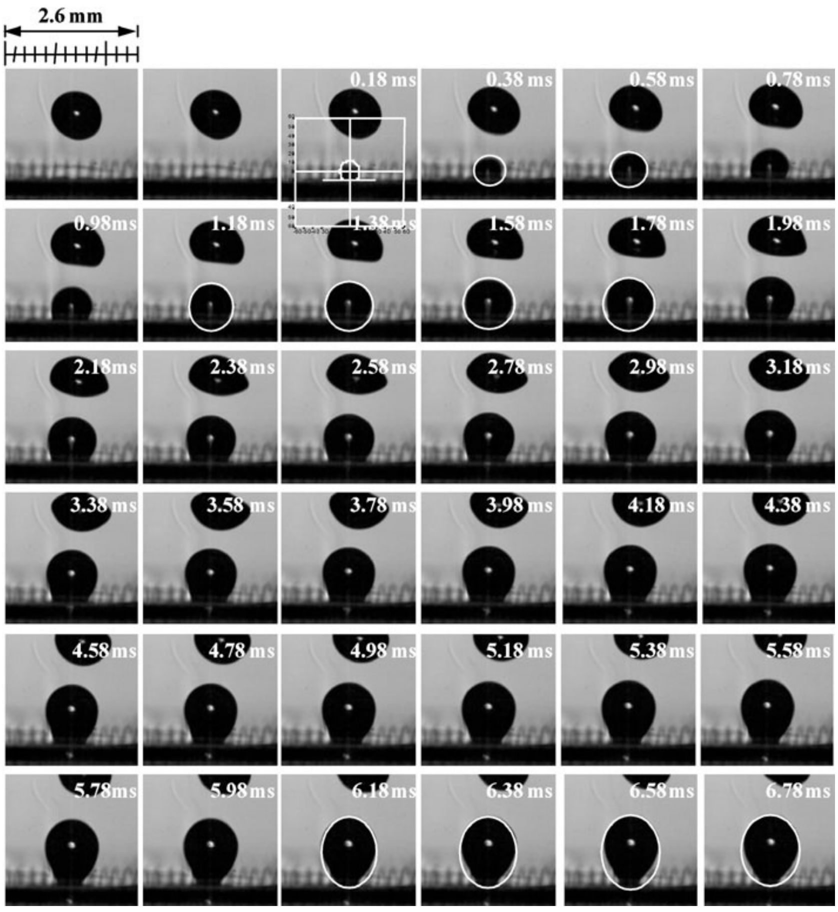

(b) T_b=47℃

Fig. 4 Side view images of bubble growth (T_b=32℃, 47℃, and 49℃)

the thermal growth region was much slower and was proportional to $t^{1/5}$, as described by Lee et al. (2003b). As based the explanation on the above, we fitted the growth equation as Eq. (9) for single bubble under saturated nucleate pool boiling of pure R113.

$$R=0.4t^{1/5}[\tanh(1.1476t^{2/3})] \tag{9}$$

The power of time for bubble growth is intimately related to the heat flow rate behavior. If the power of time for bubble growth is less than one-third, the heat flow rate described by Eq. (5) will decrease. Reversely, if the power of time for bubble growth is higher than one-third, the heat flow rate described by Eq. (5) will increase. Therefore, previous analytical results acquired from Eqs. (7), (8), and (9) showed that the heat flow rate was increased with growth time. But, during the initial growth region, when the power of the growth rate was 2/3 (see Fig. 7(a)), the heat flow rate increased with time (see Fig. 7(b)) and by contrast, during the thermal growth region, when the power of the growth rate was 1/5 (see Fig. 7 (a)), the heat flow rate decreased with time (see Fig. 7(b)) when applied Eq. (9) as the growth equation.

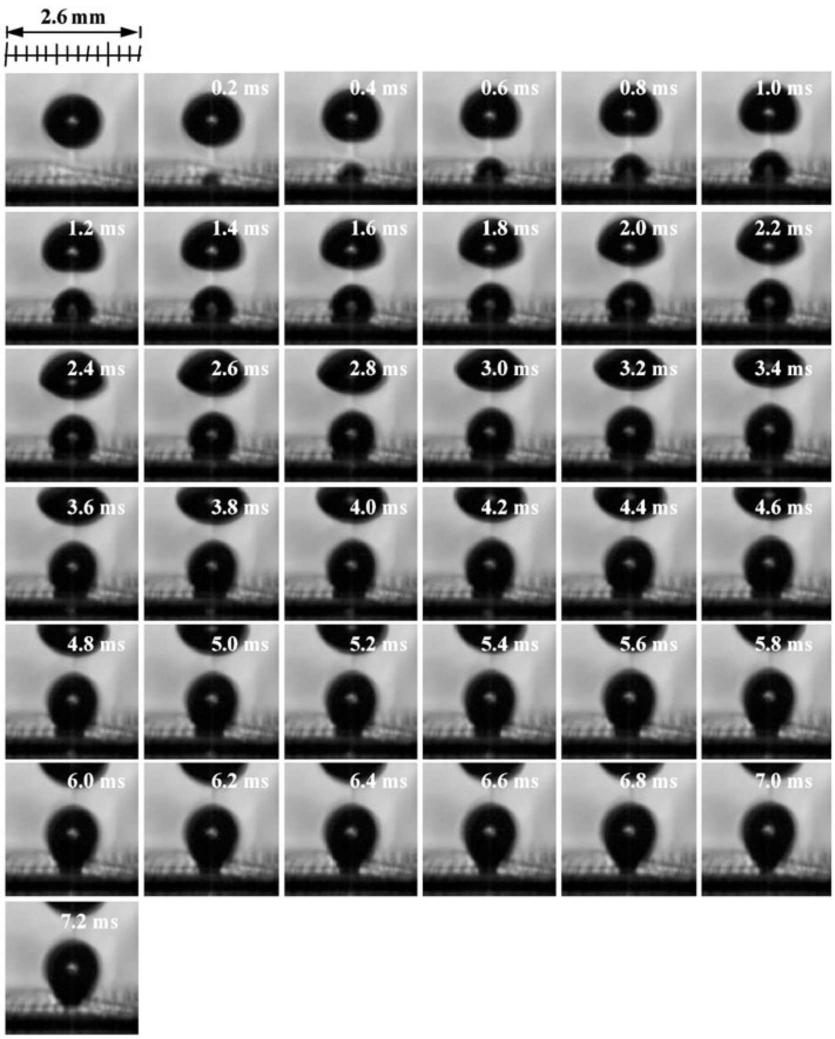

(c) T_b=49℃

Fig. 4 Side view images of bubble growth (T_b=32℃, 47℃, and 49℃)

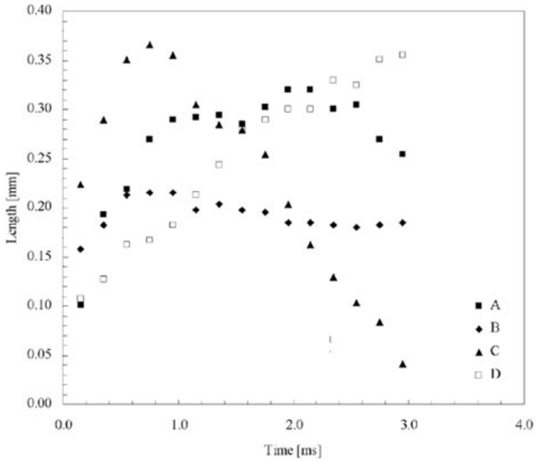

(a) $T_b=32℃$

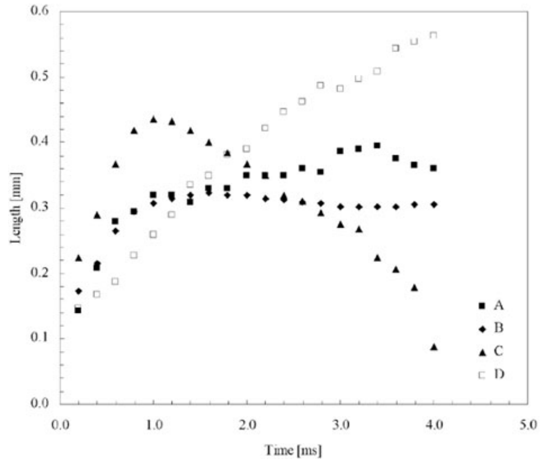

(b) $T_b=38℃$

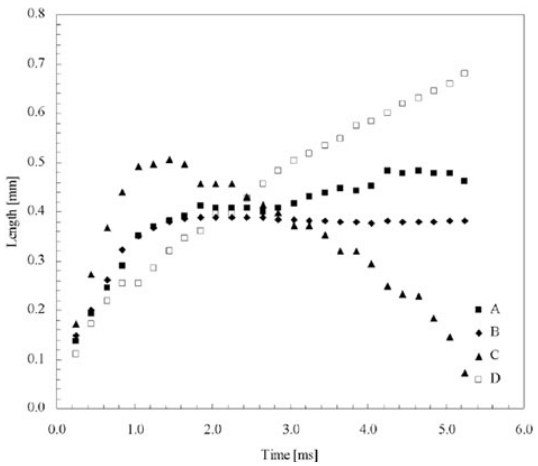

(c) $T_b=42℃$

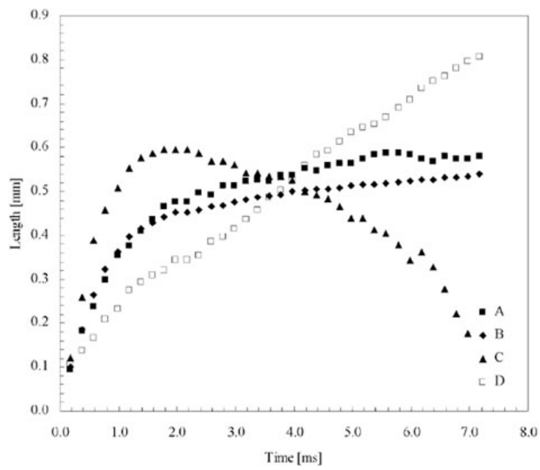

(d) $T_b=47℃$

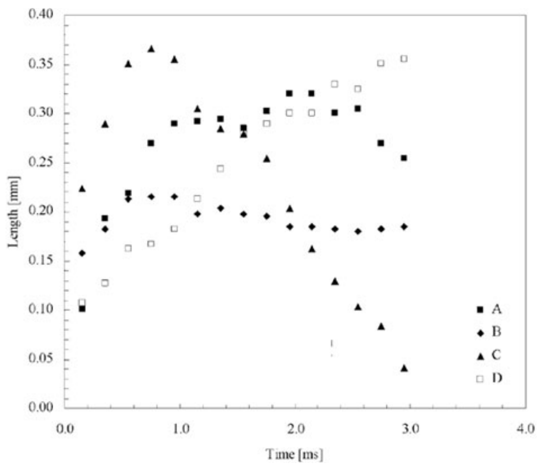

(e) $T_b=49℃$

Fig. 5 Bubble geometries for various pool conditions

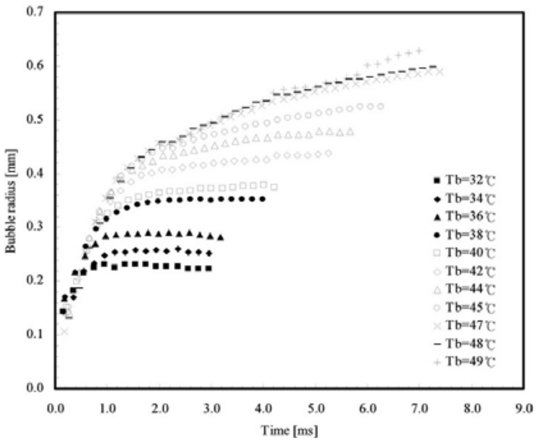

Fig. 6 Equivalent bubble radius for different pool temperatures

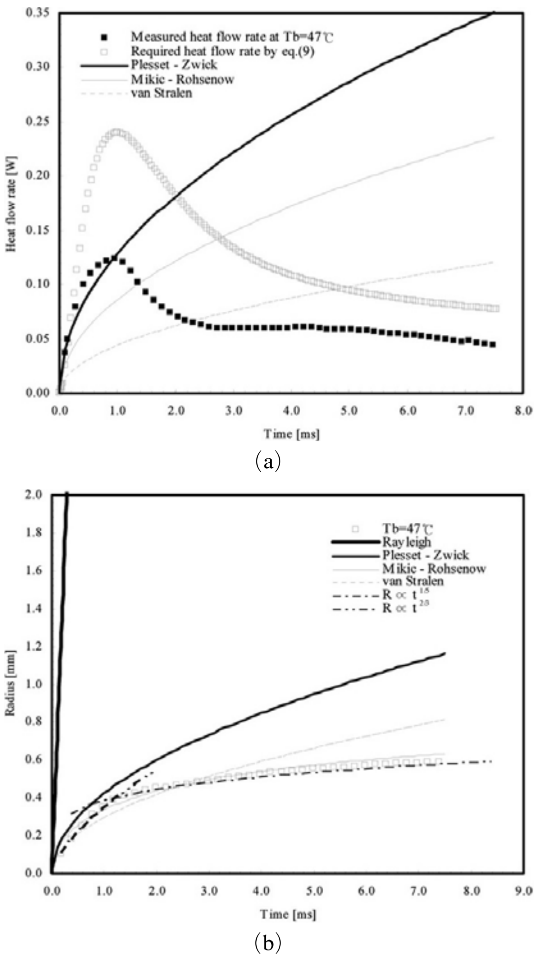

Fig. 7 Comparison of bubble growth with previous predictions (T_b=47℃)

The equivalent radius obtained for pool temperatures of 32, 38, 42, and 49℃ is compared with the analytical results of Mikic and Rohsenow (1969) and Zuber (1961) in Fig. 8. In the initial growth region, the growth rate was proportional to $t^{2/3}$, as proposed by Kim et al. (2005) for saturated pool condition. Nevertheless, the growth rate in the thermal growth region was quite different from that obtained for saturated condition.

3.2 Waiting and growth time

The waiting time was maximal for a pool temperature of 42℃, and was affected by the amount of liquid flowing into the vacant volume after departure and the temperature of that liquid flowed, as illustrated in Fig. 8. The growth time was dependent on the departure mechanism, and the departure time depended on the contact radius at departure. It was difficult to estimate the contact radius at departure because of the time gap between the capturing bubble images. Therefore, it was difficult to explain the relationship between the growth time and pool temperature. Nevertheless, as shown in Fig. 9, the growth time increased with the radius at departure time.

3.3 Dimensional analysis of the bubble growth

Suppose that the bubble growth can be characterized by the pressure difference (ΔP) between the vapor and the bulk liquid pressures. Then, the characteristic velocity scale (v_c) can be determined from the driving potential,

$$v_c = \frac{R_c}{t_c} = \sqrt{\frac{2}{3}\frac{\Delta P}{\rho_l}} \tag{10}$$

Here, the factor two-thirds is inserted to allow comparisons with the dimensionless parameter of Mikic et al. (1970).

The bubble growth behavior shown in Fig. 6 is different for each pool temperatures. We performed a dimensional analysis to compare the growth behavior with the same scales of the bubble growth, which required the characteristic time and length scales.

The characteristic time scale can be determined from the ratio of the corresponding latent heat

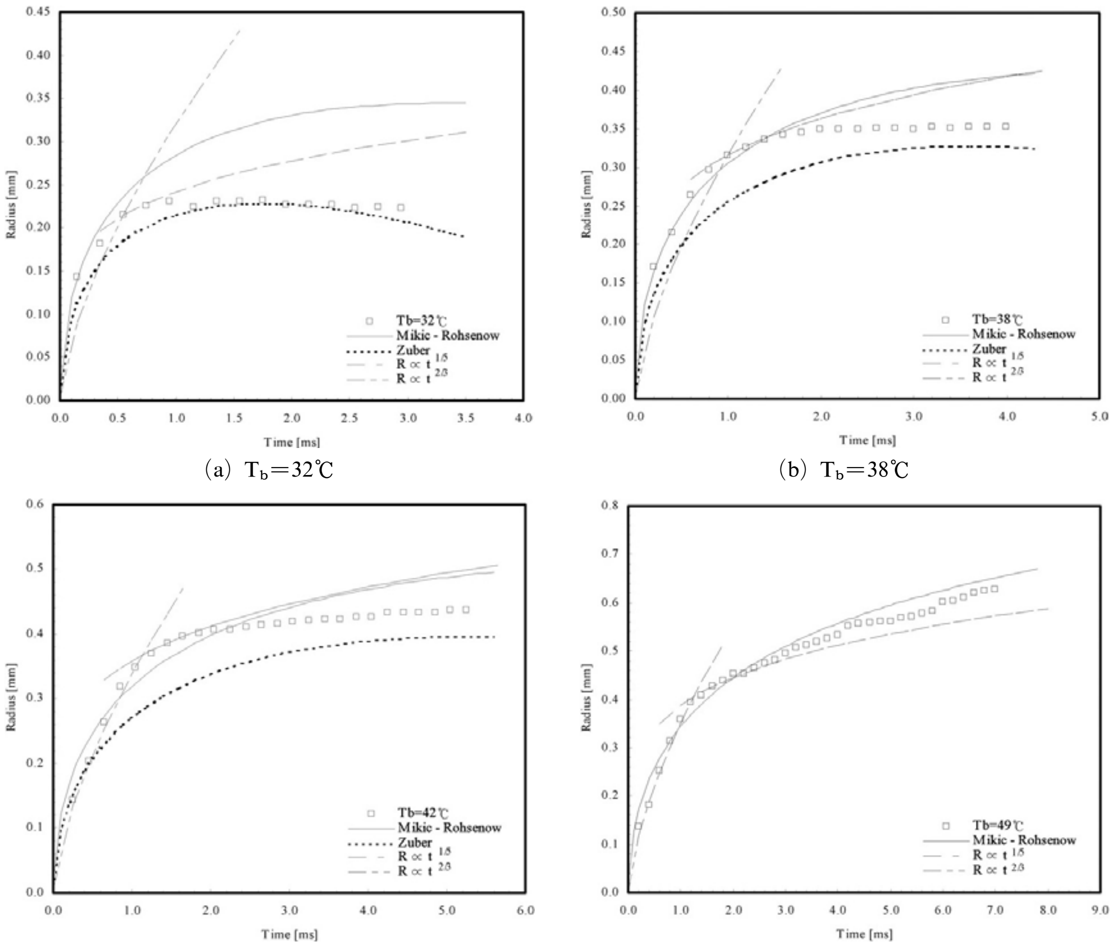

(a) T_b=32℃ (b) T_b=38℃

(c) T_b=42℃ (d) T_b=49℃

Fig. 8 Comparison of bubble growth with previous predictions (T_b=32, 38, 42, and 49℃)

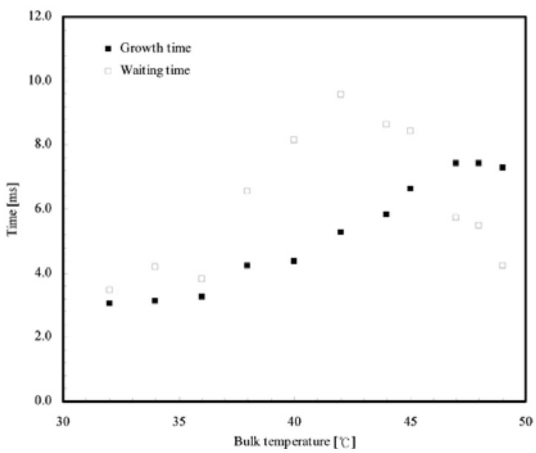

Fig. 9 Waiting and growth times for different pool temperatures

transfer and the conduction heat transfer rate through the interface,

$$\frac{q_{latent}}{\dot{q}_{conduction}}=\frac{\rho_v h_{fg}\frac{4}{3}\pi R^3}{k_l 4\pi R^2\frac{\partial T}{\partial r}} \tag{11}$$

$$=\frac{1}{3}\frac{\rho_v h_{fg}R_c^3}{k_l R_c^2\frac{T_c}{R_c}}\frac{R^{+3}}{R^{+2}\frac{\partial T^+}{\partial r^+}}=t_c\frac{R^+}{\frac{\partial T^+}{\partial r^+}}$$

$$t_c=\frac{1}{3}\frac{\rho_v h_{fg}R_c^2}{k_l T_c}$$

$$=\frac{1}{3}\frac{\rho_v h_{fg}R_c^2}{k_l\Delta T}=\frac{1}{3}\frac{1}{\mathrm{Ja}\,\alpha}R_c^2 \tag{12}$$

Since the bulk liquid is saturated and bubble growth should be influenced by the wall superheat, the Jakob number is defined by $(\rho_l C_{P_l} \Delta T)/(\rho_v h_{fg})$, where the wall superheat ($\Delta T = T_{wall} - T_{sat}$) is used as the characteristic temperature scale (T_c).

From Eqs. (10) and (12), the characteristic radius and time scales are

$$R_c = \sqrt{\frac{27}{2}}\text{Ja}\,\alpha\sqrt{\frac{\rho l}{\Delta P}},\ t_c = \frac{9}{2}\text{Ja}\,\alpha\frac{\rho_l}{\Delta P} \quad (13)$$

Then, the dimensionless bubble radius and time can be expressed as

$$R^+ = \frac{R}{R_c},\ t^+ = \frac{t}{t_c} \quad (14)$$

Mikic et al. (1970) assumed that bubble motion is governed by the extended Rayleigh equation,

$$\begin{aligned}\Delta P &= P_v - P_\infty \\ &= \rho_l R\frac{d^2R}{dt^2} + \frac{3}{2}\rho l\left(\frac{dR}{dt}\right)^2 + \frac{2\sigma}{R}\end{aligned} \quad (15)$$

By comparing the pressure difference and the second term on the right hand side of the equation, the same characteristic velocity scale can be derived. Furthermore, Mikic et al. (1970) assumed that the pressure difference was constant, and can be replaced by the superheat using the Clausius-Clapeyron relation,

$$v_c = \frac{R_c}{t_c} = \sqrt{\frac{2}{3}\frac{\Delta P}{\rho_l}} = \sqrt{\frac{2}{3}\frac{\rho_v h_{fg}\Delta T}{\rho_l T_{sat}}} \quad (16)$$

where the growth rate of Plesset and Zwick (1954) was also used for the characteristic scale. This suggests the following parameters :

$$R_c = \frac{\frac{12}{\pi}\text{Ja}^2\,\alpha}{\sqrt{\frac{\pi}{7}\frac{\rho_v h_{fg}\Delta T}{\rho_l T_{sat}}}},\ t_c = \frac{\frac{12}{\pi}\text{Ja}^2\,\alpha}{\frac{\pi}{7}\frac{\rho_v h_{fg}\Delta T}{\rho_l T_{sat}}} \quad (17)$$

It is of interest to note that almost the same relation as Mikic's scaling parameters shown above can be obtained when the critical bubble radius is used to determine the pressure difference in Eq. (16). The critical radius can be obtained using the Clausius-Clapeyron relation and the Laplace-Kelvin equation for static equilibrium. Therefore, the scaling parameters in Eq. (17) adequately describe the initial growth behavior, but not the asymptotic behavior (in the thermal controlled region).

We will use the departing radius as a scaling parameter to adjust for the thermal growth behavior. The pressure difference can be related to the departing radius, R_d, using the static equilibrium since the radial acceleration and velocity are negligible close to the bubble departure (see Eq. (15)).

Therefore,

$$\Delta P = \frac{2\sigma}{R_d} \quad (18)$$

Then, the characteristic scales from Eq. (13) can be rewritten as

$$R_c = \frac{\sqrt{27}}{2}\text{Ja}\,\alpha\sqrt{\frac{\rho_l R_d}{\sigma}},\ t_c = \frac{9}{4}\text{Ja}\,\alpha\frac{\rho_l R_d}{\sigma} \quad (19)$$

3.4 Bubble growth and heat flow rate behavior

Since the wall temperature was fixed, the Jakob numbers based on the wall and saturation temperatures for all pool temperatures were fixed at 32.4. The characteristic radius and time scales also remained constant for different pool temperatures. These were estimated using Eqn. (17) and (19) for the initial and thermal growth regions, respectively. For saturated condition of a pool temperature of 47℃, the initial region corresponded to the 1 msec from inception based on the definition proposed by Kim et al. (2005). Fig. 10(a) and (b) showed the dimensionless bubble radius characteristics as functions of the dimensionless time calculated using the estimated characteristic scales using Eqs. (19) and (17), respectively.

The bubble growth rate remained similar for the initial growth region, regardless of the pool temperature. The dimensionless bubble radius (R^+) was proportional to the dimensionless time $t^{+2/3}$, except for pool temperatures less than 40℃, for which the growth rate decreased from $t^{+2/3}$ to $t^{+1/2}$, as shown in Fig. 10(a). This indicates that a characteristic temperature scale that considers the wall and saturation temperatures can describe the initial growth behavior well. For the thermal growth region at a pool temperature of 47℃, the dimensionless radius R^+ was proportional to dimensionless time $t^{+0.216}$, as expected. The bubble

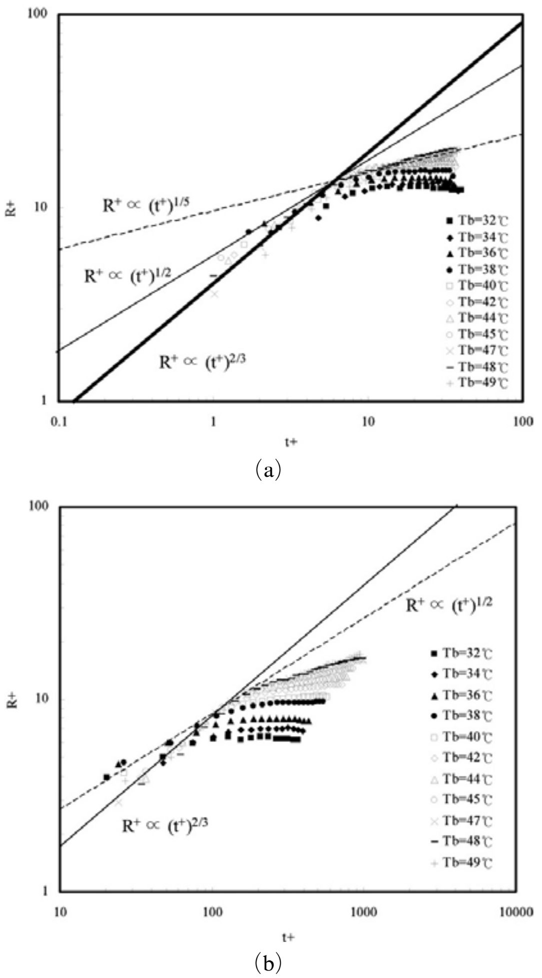

Fig. 10 Bubble growth behavior based on dimensionless scales

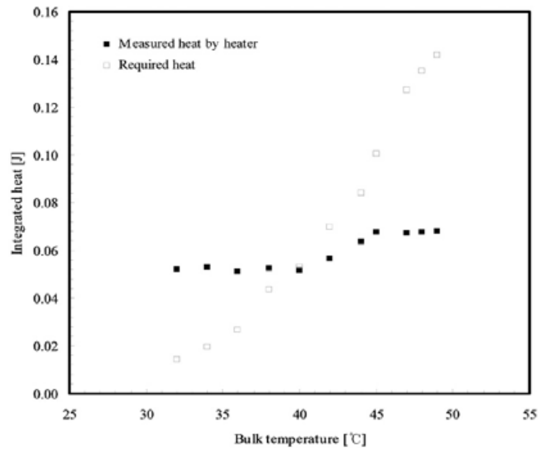

Fig. 11 Heat comparison between measured at wall and required

growth rates at pool temperatures of 48 and 49℃ were proportional to $t^{+0.224}$ and $t^{+0.263}$, respectively, as shown in Fig. 10(b). Nevertheless, these growth rates were still less than $t^{+1/3}$, so the heat flow rate behavior will decrease with growth time, as shown in Fig. 3.

We calculated the required heat flow rate for bubble growth using Eq. (5), and fitted the growth equations for each pool conditions. Then, we integrated the required and measured heat flow rates from inception to departure. The difference between the required and measured heat is shown in Fig. 11. The measured heat was defined as that which was measured using the microscale heater array to maintain the heating surface temperature at a fixed value. When the required heat was less than the measured heat, heat transfer (condensation) loss to the surrounding liquid through the bubble interface occurred at the bubble interface. This decreased bubble size and the required heat flow rate could be much less than the measured heat flow rate for low pool temperatures. When the required heat was greater than the measured heat, heat transfer from the surrounding liquid to the bubble occurred at the bubble interface, providing an interface cooling effect, as proposed by Robinson and Judd (2001). In our experiments, the required and measured heat was balanced when the pool temperature was 40℃.

We normalized the heat supplied from the heating wall using the total required heat flow rate. As shown in Fig. 12, the heat supplied from the heating wall was roughly 100, 50, and 44% of the required heat for bubble growth for pool temperatures of 40, 47, and 49℃, respectively. Therefore, when the pool temperature was increased, the contribution of the instantaneous heat supply from the wall decreased due to more heat supply (or less heat loss) from the surroun ding liquid to the bubble. For the saturation temperature, the result was similar with that of Lee et al.(2003b).

Koffman and Plesset (1983) reported that a maximum of 50% of the heat flow during bubble growth was transferred due to microlayer evapo-

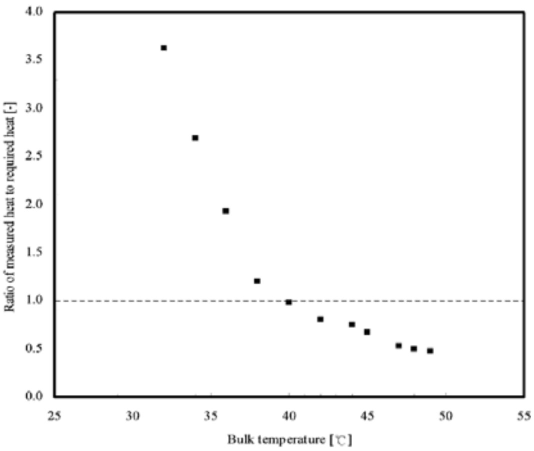

Fig. 12 Comparison of normalized heat between the measured at wall and the required

ration at saturated pool condition. From the bottom view image and heat flow rate data, we observed that the instantaneous heat was transferred through a narrow region near the contact line. Therefore, if a microlayer exists underneath the bubble, most of the measured heat flow rate supplied from the wall will be transferred by microlayer evaporation and Lee et al. (2003b) also presented similar results. Additional information about the heat transfer characteristics during single bubble growth presented here can be found in Lee et al. (2003b).

Finally, how to achieve the uniformity of temperature of the test plate during the operation can be possible through using the controller with high speed and analyzing the relation between microscale heater array geometry and bubble geometry measured.

The microscale heater array consisted of 96 microscale heaters comprised was precisely and simultaneously calibrated for each wall temperature before nucleate pool boiling. Each microscale heater measured $0.27\times0.27\ mm^2$, and the total size of the microscale heater array was $2.7\times2.7\ mm^2$. In case of the microscale heater array used in this study and fabricated by SAIT, the defected heaters was 4 heaters of 96 microscale heaters. But, a little error can be occurred from the defected heaters but the error will be negligible.

During growth before departing, just only one bubble was observed at near the center of the microscale heater array for all pool temperature conditions. A bubble grows 0.62 mm as maximum contact length and 0.63 mm as maximum equivalent bubble radius at 49℃ pool temperature condition. The uniform heating from the microscale heater array can be possible because maximum contact length dimension is less than the length of three microscale heaters and maximum equivalent bubble radius is less than half of the microscale heater array length.

And the other important to maintain the constant wall temperature is the control speed. Fig. 7 (b) shows an abrupt increase in the measured heat flow rate immediately after inception at 47℃ pool temperature condition. The characteristic scale of the heat flow rate was obtained from Eq. (5):

$$\dot{q}_c=4\pi\rho_v h_{fg} R_c^2 \frac{R_c}{t_c} \tag{20}$$

Using the characteristic scales of Eq. (19), the dimensionless heat flow rate can be expressed like Eq. (21).

$$\dot{q}_c=54\frac{1}{\sqrt{3}}\pi\rho_v h_{fg}\mathrm{Ja}^2\alpha^2\sqrt{\frac{\rho_l R_d}{\sigma}} \qquad \dot{q}^+=\frac{\dot{q}}{\dot{q}_c} \tag{21}$$

The slope of the measured dimensionless heat flow rate is about 16. Then, the variation of the characteristic time (Δt^+) for the unit change of the characteristic heat flow rate is 1/16,

$$\Delta t=t_c\Delta t^+=\frac{9}{4}\mathrm{Ja}\,\alpha\frac{\rho_l R_d}{\sigma}\times\frac{1}{16} \tag{22}$$

Using Eq. (22), the evaluated and required time variation for the unit change in the heat flow rate is 3.4×10^{-6} (0.294 MHz). Therefore, the time resolution of the heating control should be greater than this value to maintain accurate control during the rapid increase of the heat flow rate. In the present study, the oscillator of 4 MHz was used for the clock signal. Then the maximum clock speed is 2MHz (half of the oscillator speed) in this A/D system. So, the real control speed used in this study is greater than the required speed.

4. Conclusions

Through the first precise quantitative analysis of single bubble growth during subcooled, saturated, and superheated nucleate pool boiling using pure R113 with a fixed constant wall temperature, firstly the bubble shapes showed almost spheroidal shape during growth regardless of pool temperature.

The bubble growth rate remained similar for the initial growth region, regardless of the pool temperature. The dimensionless bubble radius (R^+) was proportional to the dimensionless time $t^{+2/3}$, except for pool temperatures less than 40℃, for which the growth rate decreased from $t^{+2/3}$ to $t^{+1/2}$. For the thermal growth region at a pool temperature of 47℃, the dimensionless radius R^+ was proportional to dimensionless time $t^{+0.216}$, as expected. The bubble growth rates at pool temperatures of 48 and 49℃ were proportional to $t^{+0.224}$ and $t^{+0.263}$, respectively. Nevertheless, these growth rates were still less than $t^{+1/3}$, so the heat flow rate behavior will decrease with growth time. And the bubble collapse (bubble volume decrease) of R113 was occurred at over 10℃ subcooling during attached to the heating wall.

Using our measured results, we showed the required and measured heat flow rate characteristics for all pool temperature conditions. The heat supplied from the heating wall was roughly 100, 50, and 44% of the required heat for bubble growth for pool temperatures of 40, 47, and 49℃, respectively. Therefore, when the pool temperature was increased, the contribution of the instantaneous heat supply from the wall decreased due to more heat supply (or less heat loss) from the surrounding liquid to the bubble.

Acknowledgments

This work was supported by the Ministry of Science and Technology of Korea through the National Research Laboratory program. The authors thank Prof. Jungho Kim and Dr. Sung Won Bae for providing the basic design of the microscale heater array, including its controller, and the Samsung Advanced Institute of Technology for fabricating the microscale heater array.

References

Bae, S. W., Kim, J. and Kim, M. H., 1999, "Improved Technique to Measure Time- and Space-Resolved Heat Transfer under Single Bubbles during Saturated Pool Boiling of FC-72," *Experimental Heat Transfer*, Vol. 12, No. 3, pp. 265～279.

Cole, R. and Shulman, H. L., 1966, "Bubble Growth Rates at High Jakob Numbers," *Int. J. Heat Mass Transfer*, Vol. 9, pp. 1377～1390.

Coleman, W. H. and Steele, W. G., 1989, "Experimentation and Uncertainty Analysis for Engineers," *John Wiley & Sons*.

Demiray, F. and Kim, J., 2003, "Heat Transfer from a Single Nucleation Site during Pool Boiling of FC-72," *Int. Conf. of Boiling Heat Transfer*.

Dergarabedian, P., 1960, "Observations on Bubble Growths in Various Superheated Liquids," *J. of Fluid Mechanics*, Vol. 9, pp. 39～48.

Forster, H. K. and Zuber, N., 1954, "Growth of a Vapor Bubble in a Superheated Liquid," *Journal of Applied Physics*, Vol. 25, pp. 474～478.

Han, C. H. and Griffith, P., 1965, "The Mechanism of Heat Transfer in Nucleate Pool Boiling-Part I Bubble Initiation, Growth and Departure," *Int. J. Heat Mass Transfer*, Vol. 8, pp. 887～904.

Hooper, F. C. and Abdelmessih, A. H., 1966, 3rd Intl. Heat Tr. Conf. Chicago. ; This paper is cited "A Theoretical Study on Bubble Growth in Constant and Time-Dependent Pressure Fields" by T. Theofanous, L. Biasi, H. S. Isbin and H. Fauske, 1969, Chemical Engineering Science, Vol. 24, pp. 885～897.

Kim, J., Benton, J. F. and Wisniewski, D., 2002, "Pool Boiling Heat Transfer on Small Heaters : Effect of Gravity and Subcooling," *Int. J. of Heat and Mass Transfer*, Vol. 45, pp. 3919～3932.

Kim, J., Lee, H. C., Oh, B. D. and Kim, M. H., 2004, "Effects of Bubble Shape Assumption on Single Bubble Growth Behavior in Nucleate Pool Boiling," *J. of Flow Visualization and Image*

Processing, Vol. 11, No. 1, pp. 73～87.

Kim, J., Lee, H. C., Oh, B. D. and Kim, M. H., 2005, "Study on the Single Bubble Growth During Nucleate Boiling at Saturated Pool," *KSME Series (B)*, Vol. 29, No. 2, pp. 169～179.

Koffman, L. D. and Plesset, M. S., 1983, "Experimental Observation of the Microlayer in Vapor Bubble Growth on a Heated Solid," *Journal of Heat Transfer*, Vol. 105, pp. 625～632.

Lee, H. C., Kim, J., Oh, B. D. and Kim, M. H., 2004, "Single Bubble Growth in Saturated Pool Boiling of Binary Mixtues," *Int. J. of Multiphase Flow*, Vol. 30, No. 6, pp. 697～710.

Lee, H. C., Oh, B. D., Bae, S. W., Kim, M. H., Lee, J. Y. and Song, I. S., 2003a, "Partial Nucleate Boiling on the Microscale Heater Maintaining Constant Wall Temperature," *J. of Nuclear Science and Technology*, Vol. 40, No. 10, pp. 768～774.

Lee, H. C., Oh, B. D., Bae, S. W. and Kim, M. H., 2003b, "Single Bubble Growth in Saturated Pool Boiling on a Constant Wall Temperature Surface," *Int. J. of Multiphase Flow*, Vol. 29, No. 12, pp. 1857～1874.

Lien, Y., 1969, "Bubble Growth Rates at Reduced Pressure," ScDr. Thesis, Mech. Engineering Dept., MIT.

Mikic, B. B. and Rohsenow, W. M., 1969, "Bubble Growth Rates in Non-Uniform Temperature Field," *Progress in Heat and Mass Transfer II*, pp. 283～293.

Mikic, B. B., Rohsenow, W. M. and Griffith, P., 1970, "On Bubble Growth Rates," *Int. J. Heat Mass Transfer*, Vol. 13, pp. 657～666.

Plesset, M. S. and Zwick, S. A., 1954, "The Growth of Vapor Bubbles in Superheated Liquids," *J. of Applied Physics*, Vol. 25, No. 4, pp. 493～500.

Rayleigh, J. W. S., 1917, "On the Pressure Developed in a Liquid during the Collapse of a Spherical Cavity," *Philos. Mag.*, Vol. 34, pp. 94～98. ; This is cited in the book titled "Boiling Phenomena" by S. Van Stralen (1979), McGraw-Hill.

Robinson, A. J. and Judd, R. L., 2001, "Bubble Growth in a Uniform and Spatially Distributed Temperature Field," *Int. J. of Heat and Mass Transfer*, Vol. 44, pp. 2699～2710.

Rule, T. D. and Kim, J., 1999, "Heat Transfer Behavior on Small Horizontal Heaters during Pool Boiling," *J. of Heat Transfer*, Vol. 121, No. 2, pp. 386～393.

Rule, T. D., Kim, J. and Kalkur, T. S., 1998, "Design, Construction and Qualification of a Microscale Heater Array for Use in Boiling Heat Transfer," NASA/CR-1998-207407.

Saddy, M. and Jameson, G. J., 1971, "Prediction of Departure Diameter and Bubble Frequency in Nucleate Boiling in Uniformly Superheated Liquids," *Int. J. of Heat and Mass Transfer*, Vol. 14, pp. 1771～1783.

Sernas, V. and Hooper, F. C., 1969, "The Initial Vapor Bubble Growth on a Heated Wall During Nucleate Boiling," *Int. J. Heat Mass Transfer*, Vol. 12, pp. 1627～1639.

Van Stralen S. J. D., 1966, "The Mechanism of Nucleate Boiling in Pure Liquids and in Binary Mixtures-part I," *Int. J. Heat Mass Transfer*, Vol. 9, pp. 995～1020.

Van Stralen, S. J. D., Sohal, M. S., Cole, R. and Sluyter, W. M., 1975, "Bubble Growth Rates in Pure and Binary Systems : Combined Effect of Relaxation and Evaporation Microlayers," *Int. J. Heat Mass Transfer*, Vol. 18, pp. 453～467.

Zuber, N., 1961, "The Dynamics of Vapor Bubbles in Nonuniform Temperature Fields," *Int. J. Heat Mass Transfer*, Vol. 2, pp. 83～98.